

# Quark mass effects in octet baryon magnetic polarisabilities via lattice QCD

Thomas Kabelitz, Waseem Kamleh, and Derek Leinweber

*Special Research Centre for the Subatomic Structure of Matter (CSSM),*

*Department of Physics, University of Adelaide, Adelaide, South Australia 5005, Australia*

(Dated: October 22, 2024)

The quark mass dependence of octet baryon magnetic polarisabilities is examined at the level of individual quark-sector contributions in the uniform background-field approach of lattice QCD. The aim is to understand the direct impact of increasing the mass of a quark flavour on the magnetic polarisability and indirect or environmental effects associated with changing the mass of spectator quarks, insensitive to the background magnetic field. Noting the need to set the electric charge of some quark flavours to zero, a fractionally charged baryon formalism is introduced. We find that increasing the mass of the charged quark flavour directly causes its contribution to the magnetic polarisability to decrease. However, increasing the mass of the spectator quark flavour indirectly acts to increase the magnetic polarisability. To gain a deeper understanding of these effects, we evaluate the predictions of the constituent quark model in this context. While the model provides a compelling explanation for the environmental effect of varying the spectator quark mass, an explanation of the direct mass dependence is more complicated as competing factors combine in the final result. The lattice results indicate the key factor is a reduction in the constituent quark magnetic moment with increasing quark mass, as it governs the strength of the magnetic transition to the nearby decuplet baryon.

PACS numbers: 13.40.-f, 12.38.Gc

## I. INTRODUCTION

Understanding the manner in which individual quark sectors contribute to QCD observables provides a deep understanding of QCD dynamics. The isolation of quark sectors arises naturally in theoretical calculations as one considers the coupling of a probing current to each of the quarks in turn. By effectively setting the charge of all but one quark sector to zero, one can disclose the contribution of a single quark sector.

With a quark sector isolated, one can then unravel the relationship between direct effects and indirect effects due to changes in the environment in which the selected quark flavour resides. For example, consider the  $u$ -quark sector within the proton, isolated by setting the electric charge of the  $d$ -quark to zero. One can then probe the manner in which the  $u$ -sector contribution to a proton electromagnetic observable changes as the  $u$ -quark mass is changed. Herein, we will refer to such effects as a "direct" effect. However, "indirect" effects associated with changes in the  $d$ -quark mass are also observable. We refer to such indirect effects as "environmental" effects, as the environment in which the  $u$ -quark resides changes.

Direct and indirect environmental effects in the electromagnetic form factors of octet baryons [1], decuplet baryons [2] and their transitions [3], were discovered long ago. For magnetic moments, the discovery of environmental effects was surprising as a basic tenant of the constituent quark model is a constituent quark has an intrinsic magnetic moment governed solely by its mass. There is no scope for an environmental dependence. However, such a dependence could explain violations in magnetic moment sum rules [4] and it is central to early precise predictions of the strange quark contribution to the pro-

ton's magnetic moment [5], predictions that have withstood the tests of modern determinations more than a decade later [6, 7].

In this article we present the first examination of quark-sector contributions to octet baryon magnetic polarisabilities. We explore both direct and indirect environmental effects through the variation of the masses of the quark flavours under consideration. Noting the need to set the electric charge of some quark flavours to zero, a fractionally charged baryon formalism is introduced to the background-field formalism.

In the process of understanding the underlying mechanisms that may be responsible to the effects observed in our lattice QCD calculations, we refer to the constituent quark model [8], improved to approximate recent lattice QCD results for octet baryons [9].

There the model highlights the importance of the  $u$  quark in generating a large magnetic polarisability and the impact of the octet-decuplet mass difference which suppresses the nucleon magnetic polarisabilities relative to the hyperons, especially the  $\Xi^0$ . However, there are more subtle discrepancies that remain to be understood. For example, the subtle differences that order the  $p$ ,  $n$ , and  $\Sigma^+$  magnetic polarisabilities are not fully captured in the simple model.

In this work, we aim to understand the direct and indirect effects in quark mass changes, to elucidate the role of environmental effects in QCD [10]. We aim to understand the extent to which the current simple quark model contains environmental effects and explore a possible role for additional effects that are yet to be considered in the model.

Our approach is via lattice QCD, building upon the established background field formalism. We will build on the advanced lattice techniques established in Ref. [9],

TABLE I. The properties of the four quark flavours considered in isolating individual quark-sector contributions to baryon magnetic polarisabilities.

Quark	Symbol	Electric Charge	Mass
down	$d$	$-1/3$	$m_d$
strange	$s$	$-1/3$	$m_s$
light	$l$	$0$	$m_d$
heavy	$h$	$0$	$m_s$

this time neutralising quark sectors to access the contributions one flavour at a time. We will carefully examine the direct and indirect effects through both lattice QCD and the constituent quark model, allowing a determination of the capability of the constituent quark model and the opportunity to evaluate whether environmental effects are as relevant for the magnetic polarisability as they are for the magnetic moment.

In Sec. II we define a fractionally charged baryon formalism that enables an examination of direct and indirect environment effects. In Sec. III we briefly revisit the magnetic polarisability in the constituent quark model before we consider its predictions for fractionally charged baryons. In Sec. IV we review our implementation of the background field method. The extraction of the magnetic polarisability on the lattice is presented in Sec. V. In Sec. VI we discuss our fitting methodology and treatment of excited state contamination of the underlying correlation functions required to extract the magnetic polarisability in the background field method. The details of the lattice simulation are presented in Sec. VII. In Sec. VIII we present our results of the lattice simulation and evaluate the quark model's ability to describe them. In Sec. IX we summarise our findings.

## II. FRACTIONALLY CHARGED BARYONS

We begin by defining a formalism in which we can probe the direct and indirect environmental effects of quark mass changes in the magnetic polarisabilities of octet baryons. As in Ref. [9], we consider the outer members of the baryon octet to avoid issues with the mixing of  $\Sigma^0$  and  $\Lambda$  baryons in the background field. As such, the quantum numbers of these baryons are carried by two quark flavours. We are specifically interested in two concepts.

*Direct quark mass dependence:* How the contribution of a quark sector changes as its mass changes between that of a down quark and that of a strange quark (e.g.  $d \rightarrow s$  in  $n \rightarrow \Xi^0$ ).

*Indirect environmental dependence:* How the contribution of a quark sector changes as the mass of the other sector changes between that of a down and strange quark (e.g.  $u$  in  $p \rightarrow \Sigma^+$ ).

We determine these contributions by constructing

baryons with a single electrically charged flavour and a neutrally charged flavour, thereby isolating the electrically charged flavour's contribution. To do so we utilise the four quark flavours defined in Table I and construct eight baryons with the flavours

$$\begin{array}{cccc} ddl, & lld, & ssl, & lls, \\ ddh, & hhd, & ssh, & hhs. \end{array}$$

These eight baryons allow us to examine the direct quark mass dependence

$$\begin{aligned} ddl &\rightarrow ssl, \\ ddh &\rightarrow ssh, \\ lld &\rightarrow lls, \\ hhd &\rightarrow hhs, \end{aligned} \quad (1)$$

and the indirect environment dependence

$$\begin{aligned} ddl &\rightarrow ddh, \\ ssl &\rightarrow ssh, \\ lld &\rightarrow hhd, \\ lls &\rightarrow hhs, \end{aligned} \quad (2)$$

of all possible charge and environment sectors. To examine the direct and environmental dependence, we examine differences in the magnetic polarisability such as  $\beta_{ssl} - \beta_{ddl}$  for the direct mass effect. In calculating the difference, we will take advantage of correlations between the quantities to accurately discern changes due to variation of the quark masses.

## III. CONSTITUENT QUARK MODEL

In a simple constituent quark model, the constituent quark masses are tuned to reproduce the magnetic moments of the  $p$ ,  $n$ , and  $\Lambda$  baryons [11]. Such a simple model relies on the assumption that the quarks are blind to their environment. For example, this assumption makes the contribution of the  $u$  quark the same in the  $n$  ( $ddu$ ) and the  $\Xi^0$  ( $ssu$ ), despite the change in the mass of its environment. However, experimental evidence of environmental effects was highlighted in Ref. [5] for the magnetic moments. Nonetheless, the constituent quark model retains significant value. Its ability to simply describe the qualitative pattern exhibited by the baryon magnetic moments is complemented by a remarkable ability to explain the broad behaviours of the magnetic polarisability of the octet baryons as presented in Ref. [9].

In that work we derived the following expression for the magnetic polarisability of an outer octet baryon

$$\begin{aligned} \beta &= \frac{1}{2\pi} \frac{|\langle \mathcal{B} | \hat{\mu}_z | \mathcal{B}^* \rangle|^2}{m_{\mathcal{B}^*} - m_{\mathcal{B}}} - \sum_{f=1}^3 \frac{q_f^2 \alpha}{6m_f} \langle r^2 \rangle_f, \\ &= \frac{4}{9\pi} \frac{|\mu_D - \mu_S|^2}{m_{\mathcal{B}^*} - m_{\mathcal{B}}} - \sum_{f=1}^3 \frac{q_f^2 \alpha}{6m_f} \langle r^2 \rangle_f, \\ &\equiv \beta_1 - \beta_2, \end{aligned} \quad (3)$$

where  $\alpha = e^2/4\pi$  is the fine structure constant.  $\beta_1$  depends on the magnetic transition moment between octet and decuplet baryons for the outer members of the baryon octet

$$\langle \mathcal{B} | \hat{\mu}_z | \mathcal{B}^* \rangle = \frac{2\sqrt{2}}{3} (\mu_D - \mu_S), \quad (4)$$

expressed in terms of the constituent quark moments of the doubly,  $\mu_D$ , and singly,  $\mu_S$ , represented sectors for an outer octet baryon. In the constituent quark model, the constituent quark moments are given in terms of the constituent quark masses,  $m_f$ , for each flavour,  $f$

$$\mu_f = \frac{q_f e}{2 m_f}. \quad (5)$$

The contributions of opposing sign in Eq. (3) produce interesting complexity [9].  $\beta_1$  probes the transition to an intermediate excitation through virtual photon exchange, while  $\beta_2$  probes the distribution of quarks within the hadron.

### A. Implementing the quark model

The quark model predictions require the model's input quantities be determined on the lattice and interpolated. The details of this interpolation are described in depth in Ref. [9]. To estimate the constituent quark masses away from the physical point, we utilise a simple model

$$\begin{aligned} m_{\text{oct}}^0 + \alpha_{\text{oct}} (3 m_l) &= m_N, \\ m_{\text{oct}}^0 + \alpha_{\text{oct}} (m_l + 2 m_h) &= m_{\Xi}. \end{aligned} \quad (6)$$

Here  $m_l = m_d$  and  $m_h = m_s$  are the light and heavy constituent quark masses already determined in the simple constituent quark model via baryon magnetic moments at the physical point, as summarised in Ref. [11].  $m_{\text{oct}}^0$  and  $\alpha_{\text{oct}}$  are fit parameters, constrained by the physical nucleon and  $\Xi$  masses. With the parameters determined, one can then use Eq. (6) with baryon masses from our lattice QCD simulations to solve for the constituent quark masses,  $m_l$  and  $m_h$ , away from the physical point.

We linearly interpolate the octet baryon masses as a function of pion mass [12], allowing the determination of the constituent quark masses as a function of the pion mass.

In the spirit of the constituent quark model, we utilise these constituent quark masses and equations of the form Eq. (6) to determine the octet baryon masses, including the masses of fractionally charged baryons that would otherwise not exist. This includes the mass of an octet  $ssh$  or  $hhs$  with a mass of

$$m_{ssh} = m_{hhs} = m_{\text{oct}}^0 + \alpha_{\text{oct}} (3 m_h). \quad (7)$$

The decuplet baryon masses are determined using an equivalent model with fit parameters determined in the

same manner using the same physical point  $m_l$  and  $m_h$  constituent quark masses, and the physical  $\Delta$  and  $\Omega$  masses.

Finally, we interpolate the quark distribution radii determined on the PACS-CS ensembles by Stokes *et al.* [13]. The proton and neutron squared radii are characterised well with an interpolation that is linear in  $\log(m_\pi)$ . Quark distribution radii for single quark flavours of unit charge in the doubly ( $D$ ), and singly ( $S$ ), represented sectors are defined by

$$\langle r^2 \rangle_p = 2 \frac{2}{3} \langle r^2 \rangle_D - \frac{1}{3} \langle r^2 \rangle_S, \quad (8)$$

$$\langle r^2 \rangle_n = -2 \frac{1}{3} \langle r^2 \rangle_D + \frac{2}{3} \langle r^2 \rangle_S, \quad (9)$$

where charge and quark-counting factors are explicit. The resulting distribution radii for single quarks of unit charge are

$$\langle r^2 \rangle_D = \frac{1}{2} (2 \langle r^2 \rangle_p + \langle r^2 \rangle_n), \quad (10)$$

$$\langle r^2 \rangle_S = \langle r^2 \rangle_p + 2 \langle r^2 \rangle_n. \quad (11)$$

As only the proton and neutron were examined in Ref. [13], we approximate the doubly and singly represented strange-quark distribution radii to be that of the light quark at the heaviest PACS-CS quark mass labelled by  $m_\pi = 701$  MeV.

### B. Constituent quark model predictions for the magnetic polarisability

Using the above implementation, the magnetic polarisability of the outer octet baryons are predicted in Ref. [9]. A simple magnitude correction is required

$$\beta = a_1 \beta_1 - a_2 \beta_2, \quad (12)$$

where the fit parameters  $a_1 = 0.401$ ,  $a_2 = 0.532$  best reproduce the lattice QCD data. The phenomenology associated with this scaling is discussed in Ref. [9]. With this improvement, the quark model is able to capture the qualitative features of the lattice QCD determinations as illustrated in Fig. 1.

Specifically, it predicts the small nature of the magnetic polarisability of the  $\Sigma^-$  and  $\Xi^-$  baryons, which was otherwise not known. It also correctly predicts the large magnetic polarisability of the  $\Xi^0$ . Finally, it predicts approximately the correct magnitude for the magnetic polarisability of the  $p$ ,  $n$ , and  $\Sigma^+$  though there is a lack of clarity about their ordering. The successes of the model are significant given its simplicity.

The model also highlights the importance of the  $u$  quark in generating a large magnetic polarisability through the transition term  $\beta_1$  with the factor  $(\mu_D - \mu_S)^2$ . Combinations of  $\mu_u$  and  $\mu_d$  or  $\mu_s$  add and square to a large magnitude, whereas a combination of  $\mu_d$  and  $\mu_s$

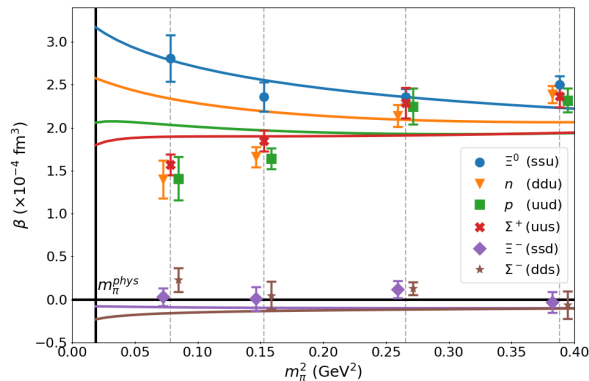


FIG. 1. Improved quark model predictions from Ref. [9] for the magnetic polarisabilities of octet baryons (curves) are compared with lattice QCD determinations (points) calculated on the PACS-CS ensembles considered herein. The legend is ordered to match the vertical ordering of the quark model curves at the physical pion mass. Dashed lines represent the pion masses of the PACS-CS ensembles.

approximately cancel and become small in the square. This latter point explains the small magnitude of the  $\Sigma^-$  and  $\Xi^-$  magnetic polarisabilities.

The more subtle discrepancies between the model and the lattice simulation results may be associated with an environmental effect in the constituent quark moments as discussed in the introduction. Thus, we turn our attention to the contributions of individual quark sectors with an aim to understanding direct and indirect environmental effects governing their contributions to the magnetic polarisability.

### C. Fractionally charged baryon formalism

We first evaluate the quark model predictions when considering fractionally charged baryons. Consider the magnetic polarisability of Eq. (3) for the proton

$$\begin{aligned} \beta_{uud} &= \frac{4}{9\pi} \frac{|\mu_u - \mu_d|^2}{m_\Delta - m_N} - \frac{8}{9} \frac{\alpha}{6 m_l} \langle r^2 \rangle_l - \frac{1}{9} \frac{\alpha}{6 m_l} \langle r^2 \rangle_l, \\ &= \frac{4}{9\pi} \frac{9\mu_d^2}{m_\Delta - m_N} - \frac{\alpha}{6 m_l} \langle r^2 \rangle_l, \end{aligned} \quad (13)$$

where we have used the charge symmetric relation  $\mu_u = -2\mu_d$ . Now consider neutralising the  $u$  quark sector for the  $lld$  baryon

$$\begin{aligned} \beta_{lld} &= \frac{4}{9\pi} \frac{|\mu_d|^2}{m_\Delta - m_N} - \frac{1}{9} \frac{\alpha}{6 m_l} \langle r^2 \rangle_l, \\ &= \frac{4}{9\pi} \frac{\mu_d^2}{m_\Delta - m_N} - \frac{1}{9} \frac{\alpha}{6 m_l} \langle r^2 \rangle_l. \end{aligned} \quad (14)$$

We note a significant drop in the magnitude by a factor of nine. Our focus on the elemental  $d$  quark in the lattice

QCD simulations means that this reduction by an order of magnitude will have significant implications that will be discussed in due course.

#### 1. Environmental dependence in the quark model

Considering the environmental dependence in  $lld \rightarrow hhd$ , we note that the charged sector is unchanged. As a result, when taking the difference

$$\beta_{hhd} - \beta_{lld} = \frac{4}{9\pi} \left[ \frac{\mu_d^2}{m_{\Sigma^*} - m_\Xi} - \frac{\mu_d^2}{m_\Delta - m_N} \right], \quad (15)$$

the quark distribution term vanishes and we are left only with the difference in the octet-decuplet mass splittings. The quark model's prediction of a nontrivial environmental effect for the magnetic polarisability contrasts that for the magnetic moment.

The result of Eq. (15) can be easily extended to the other three environmental effects of Eq. (2). In every case, there are additional heavy quarks in the right-hand baryon of Eq. (2). As hyperfine splittings are inversely proportional to the product of the constituent quark masses, the octet-decuplet mass splitting is smaller for baryons with more heavy quarks. Thus, the decuplet – octet baryon mass splitting is smaller for the leading term and the sign of all environment effects are predicted to be positive.

#### 2. Direct quark mass dependence in the quark model

In the case of the mass dependence, the mass of the charged sector is changing and the expression becomes more complex. Considering  $lld \rightarrow lls$

$$\begin{aligned} \beta_{lls} - \beta_{lld} &= \frac{4}{9\pi} \left[ \frac{\mu_s^2}{m_{\Sigma^*} - m_\Sigma} - \frac{\mu_d^2}{m_\Delta - m_N} \right] \\ &\quad - \left[ \frac{\alpha q_s^2}{6 m_h} \langle r^2 \rangle_h - \frac{\alpha q_d^2}{6 m_l} \langle r^2 \rangle_l \right], \end{aligned} \quad (16)$$

we observe none of the previous cancellation. Instead we observe competing effects.

As  $\mu_d^2 > \mu_s^2$  and  $(m_\Delta - m_N)^{-1} < (m_{\Sigma^*} - m_\Sigma)^{-1}$  the sign of the first term depends on the interplay between these two factors. However the sign of the second term is clear as  $\langle r^2 \rangle_h / m_h < \langle r^2 \rangle_l / m_l$  and thus the contribution including the leading minus sign is positive. Therefore, if  $\beta_{lls} - \beta_{lld} < 0$  then one can point to  $\mu_d^2 > \mu_s^2$  as the dominant effect.

Similar arguments hold for the case of  $hhd \rightarrow hhs$ . If  $\beta_{hhs} - \beta_{hhd} < 0$  then one can point to  $\mu_d^2 > \mu_s^2$  as the dominant effect.

Now consider  $ddl \rightarrow ssl$ ,

$$\beta_{ssl} - \beta_{ddl} = \frac{4}{9\pi} \left[ \frac{\mu_s^2}{m_{\Xi^*} - m_{\Xi}} - \frac{\mu_d^2}{m_{\Delta} - m_N} \right] - 2 \left[ \frac{\alpha q_s^2}{6 m_h} \langle r^2 \rangle_h - \frac{\alpha q_d^2}{6 m_l} \langle r^2 \rangle_l \right]. \quad (17)$$

This time the octet-decuplet mass splitting creates even greater tension between competing effects as does the charge distribution term. While  $\mu_d^2 > \mu_s^2$  as before,  $(m_{\Delta} - m_N)^{-1} \ll (m_{\Xi^*} - m_{\Xi})^{-1}$  and thus there is greater competition between the factors in setting the sign. The sign of the second term is as before, but with double the magnitude.

If  $\beta_{ssl} - \beta_{ddl} < 0$  then one can once again point to  $\mu_d^2 > \mu_s^2$  as the dominant effect. However, the quark model predicts a suppressed effect relative to  $\beta_{us} - \beta_{ud}$  due to a reduced difference in mass splittings and the magnitude of the quark distribution term.

Finally, similar arguments hold for the case of  $ddh \rightarrow ssh$ . If  $\beta_{ssh} - \beta_{ddh} < 0$  then one can point to  $\mu_d^2 > \mu_s^2$  as the dominant effect. Again the effect is predicted to be suppressed relative to  $hhd \rightarrow hhs$ .

To summarise, if the change in the constituent quark magnetic moment dominates the direct quark-mass effect, the case of  $hhd \rightarrow hhs$  holds the greatest promise for illustrating an effect in the lattice QCD simulations. The prevalence of heavy quarks will aid in suppressing statistical uncertainties and the tension between  $\mu_d^2 > \mu_s^2$  and competing effects is lowest for  $\beta_{hhs} - \beta_{hhd}$ . If  $\beta_{hhs} - \beta_{hhd} < 0$  then one has a simple intuitive picture of the physics driving the direct quark mass effect. It is the simple suppression of the constituent quark moment that suppresses transitions to nearby decuplet baryons and thus diminishes the polarisability.

We now proceed to the lattice QCD calculation to provide reference to these predictions.

#### IV. BACKGROUND FIELD IMPLEMENTATION

The background field method is a well established approach to calculating the magnetic polarisability in a lattice QCD calculation. The approach used in this work is identical to our approach in Ref. [9]. Full details are given there.

In the background field method, a minimal coupling to the discretised covariant derivative results in the application of a phase to the QCD gauge field. Through the requirement for periodicity at the boundary, we obtain a quantisation condition for the magnetic field strength  $B$  given by

$$eB = \frac{2\pi}{N_x N_y a^2} \frac{1}{q_d} k_d, \quad (18)$$

where  $k_d$  is an integer specifying the field strength in multiples of the minimum uniform field strength quantum. The condition is written in terms of the down quark

charge  $q_d e$ , the number of spatial sites  $N_x, N_y$  and the lattice spacing  $a$ .

The magnetic field is defined such that the field corresponding to integer  $k_d = 1$  is oriented in the negative  $\hat{z}$ -direction. This work utilises quark propagators and baryon correlation functions calculated at  $k_d = 0, \pm 1, \pm 2$ . We will refer to the strength of the magnetic field in terms of  $k_d$  throughout this work.

#### V. LATTICE QCD FORMALISM

In the presence of a uniform background magnetic field, the energy of a baryon changes as a function of magnetic field strength [14, 15]

$$E(B) = m + \vec{\mu} \cdot \vec{B} + \frac{|q_B e B|}{2m} (n+1) - \frac{1}{2} 4\pi \beta B^2 + \mathcal{O}(B^3). \quad (19)$$

Here the mass of the baryon,  $m$ , is complemented by contributions from the magnetic moment  $\vec{\mu}$ , the Landau term proportional to  $|q_B e B|$  where  $q_B$  is the charge of the baryon, and the magnetic polarisability  $\beta$ . As the baryons in this work are fractionally charged, we use a U(1) Landau-mode projection to select  $n = 0$ . This aspect of the calculation is detailed in Sec. VII D.

As we demonstrated in Ref. [9], the contribution from the magnetic moment may be subtracted by consideration of the average of "spin-field aligned" and "spin-field anti-aligned" energy. The baryon mass may also be removed through the subtraction of the zero-field energy.

This process may be mirrored in a correlation function ratio which enables cancellation of correlated fluctuations. We define a "spin-field aligned" correlator

$$G_{\uparrow\uparrow}(B) = G(+s, +B) + G(-s, -B), \quad (20)$$

where the baryon's spin is aligned with the magnetic field and a "spin-field anti-aligned" correlator

$$G_{\uparrow\downarrow}(B) = G(+s, -B) + G(-s, +B), \quad (21)$$

where the spin and field are opposed. These correlators are combined in the ratio

$$R(B, t) = \frac{G_{\uparrow\uparrow}(B, t) G_{\uparrow\downarrow}(B, t)}{G(0, t)^2}, \quad (22)$$

which aggregates the positive and negative field strengths together. Due to this aggregation, any reference to the magnetic field strength from this point refers to the aggregated positive field strength.

The effective energy of this correlation function ratio acts to subtract the magnetic moment term and baryon mass. As such, we define the magnetic polarisability en-

ergy shift  $\delta E_\beta(B, t)$

$$\begin{aligned}\delta E_\beta(B, t) &= \frac{1}{2} \frac{1}{\delta t} \lim_{t \rightarrow \infty} \log \left( \frac{R(B, t)}{R(B, t + \delta t)} \right), \\ &= \frac{1}{2} [\delta E_{\uparrow\uparrow}(B) + \delta E_{\uparrow\downarrow}(B)] - \delta E(0) \\ &= \frac{|q e B|}{2m} - \frac{4\pi}{2} \beta |B|^2 + \mathcal{O}(B^3).\end{aligned}\quad (23)$$

However, we require more than the magnetic polarisability of a single baryon, instead we require the difference in magnetic polarisability between two baryons. We saw in Sec. II that fractionally charged baryons have magnetic polarisabilities an order of magnitude smaller than that of the physical baryons composed with a  $u$  quark. As such, extracting sufficient signal to take a meaningful difference is difficult. Extracting the magnetic polarisability of the fractionally charged baryons separately and determining a correlated difference often fails to produce meaningful insight, especially at lighter quark masses.

However, the highly correlated nature of the two baryons can be exploited by calculating the difference at the correlator level. As such, we construct the ratio  $R(B, t)$  for both baryons in question and construct the following effective energy shift

$$\begin{aligned}\delta E_{\beta_1 - \beta_2}(B, t) &= \frac{1}{2} \frac{1}{\delta t} \lim_{t \rightarrow \infty} \log \left( \frac{R_{\beta_1}(B, t) R_{\beta_2}(B, t + \delta t)}{R_{\beta_1}(B, t + \delta t) R_{\beta_2}(B, t)} \right), \\ &= \left( \frac{|q_{B_1}|}{m_{B_1}} - \frac{|q_{B_2}|}{m_{B_2}} \right) \frac{|eB|}{2} - \frac{4\pi}{2} (\beta_1 - \beta_2) |B|^2 \\ &\quad + \mathcal{O}(B^3).\end{aligned}\quad (24)$$

This allows for fitting of the magnetic polarisability difference  $\beta_1 - \beta_2$  directly, providing maximal cancellation of correlated fluctuations. We note that the magnetic polarisability differences we are interested in here will always have  $q_{B_1} = q_{B_2}$ , hence the quark charge may be factored out of the difference in the Landau term.

## VI. FITTING

To extract the magnetic polarisability difference  $\beta_1 - \beta_2$  we fit Eq. (24) as a function of field strength. In practice, it is simpler to fit in terms of the field strength quanta  $k_d$ . Using the quantisation condition of Eq. (18)

$$eB = \frac{2\pi}{N_x N_y a^2} \frac{1}{q_d} k_d, \quad (25)$$

we substitute for  $eB$  in Eq. (24) to re-write  $\delta E_{\beta_1 - \beta_2}$  in terms of the field strength quanta

$$\delta E_{\beta_1 - \beta_2}(k_d) = L(k_d, m_{B_1}, m_{B_2}) + C (\beta_1 - \beta_2) k_d^2, \quad (26)$$

where

$$L(k_d, m_{B_1}, m_{B_2}) = \frac{1}{2} \frac{2\pi}{N_x N_y a^2} \left( \frac{|q_{B_1}|}{m_{B_1}} - \frac{|q_{B_2}|}{m_{B_2}} \right) \left| \frac{1}{q_d} k_d \right|, \quad (27)$$

and

$$C = -\frac{1}{2\alpha} \left[ \frac{2\pi}{N_x N_y a^2} \right]^2 \frac{1}{q_d^2}. \quad (28)$$

It is important to note that  $q_d$  is the down quark charge while  $q_{B_1}, q_{B_2}$  are the hadronic charges of the two baryons. For convenient future reference, we have defined  $L(k_d, m_1, m_2)$  the combined Landau contribution and  $C$  the remaining coefficient to the magnetic polarisability difference.

We fit  $\delta E_{\beta_1 - \beta_2}$  at two positive field strengths to extract the magnetic polarisability difference  $\beta_1 - \beta_2$ . We obtain the best estimate for  $\delta E_{\beta_1 - \beta_2}(k_d)$  through a weighted average of fit windows which provides a systematic approach to plateau fitting [16]. The method is detailed fully in Ref. [9].

In the method, the  $i$ th eligible window of  $N$  candidates is assigned a weight according to

$$w_i = \frac{1}{\mathcal{Z}} \frac{p_i}{(\delta E_i)^2}, \quad (29)$$

where

$$\mathcal{Z} = \sum_{i=1}^N \frac{p_i}{(\delta E_i)^2}. \quad (30)$$

Here,  $\delta E_i$  is the uncertainty of the  $i$ th fit, and  $p_i$  is the  $p$ -value of the fit. The  $p$ -value is the probability of a given fit occurring in a  $\chi^2$  distribution. With these weights, the average effective energy is

$$E = \sum_i^n w_i E_i, \quad (31)$$

and the statistical error

$$(\delta E)^2 = \sum_i^n w_i (\delta E_i)^2. \quad (32)$$

Eligible windows must satisfy a few criteria. To avoid fitting noise, we define a  $t_{\max}$ , the last time slice before signal is clearly lost to noise. We define a corresponding  $t_{\min}$ , the first time slice at which single state isolation has been reached for all underlying (spin-field aligned, anti-aligned, zero-field) correlation functions. We also require the fit window to be of minimum length three and  $t_f = t_{\max}$ . This fixing of the endpoint ensures that early time-slices are not disproportionately favoured.

In our examination of the octet baryons in Ref. [9] we found it vital to impose the condition of single state isolation on all underlying correlation functions when determining  $t_{\min}$ . In constructing the correlation function ratio Eq. (22) (which enables the extraction of the magnetic polarisability) the resulting correlator can display plateau-like behaviour before the underlying correlation functions have reached single state isolation.

As we did in that work, we utilise the  $\chi_{\text{dof}}^2$  of a linear fit to  $\log G$  as a metric for excited state contamination. An easy interface to the large number of  $\chi_{\text{dof}}^2$  to be checked are the set of heatmaps we construct for each particle. The heatmaps for the  $d\bar{d}l$  baryon at  $\kappa = 0.13700$ ,  $m_\pi = 296$  MeV are shown in Fig. 2.

We consider a correlator to have reached single state isolation when the first three windows have  $\chi_{\text{dof}}^2 < 2.5$  which corresponds to the three leftmost boxes being coloured blue, green or yellow. We can see this criteria has been fulfilled by all underlying correlation functions by  $t = 24$  for the  $d\bar{d}l$  baryon. In determination of the difference we also consider the heatmaps of the other baryon in question and set  $t_{\text{min}}$  to the larger of the two earliest times.

As shown in Sec. III C the magnetic polarisability of the fractionally charged baryons is an order of magnitude smaller than that of physical baryons. Further, we are interested in the magnetic polarisability difference. The difference is a very sensitive quantity and extracting meaningful signal is difficult, especially at light quark masses.

As a result, we will extract two sets of data in this work. One in which the underlying correlation functions are explicitly checked for single state isolation. This dataset we denote "Corr." to reflect the correlator level examination of the  $\chi_{\text{dof}}^2$ . We will also produce a dataset where this criteria is relaxed and we examine the correlated  $\chi_{\text{dof}}^2$  of the energy shift ratio to produce appropriate sampling of the possible fit windows. We denote this dataset "Ratio". In this case we set  $t_{\text{min}} = t_{\text{source}} + 2$ . We will see in the results section that the two datasets agree at  $1\sigma$ .

Having defined values for  $\delta E_{\beta_1 - \beta_2}(k_d)$  at  $k_d = 1, 2$ , we turn our attention to the Landau term  $L(k_d, m_1, m_2)$  of Eq. (26), which depends on the baryon masses. These masses are also determined through the weighted average approach. Subtraction of this known term allows the magnetic polarisability difference to be extracted as a single parameter in the fit of

$$\frac{\delta E_{\beta_1 - \beta_2}(k_d) - L(k_d, m_{B_1}, m_{B_2})}{C} = (\beta_1 - \beta_2) k_d^2. \quad (33)$$

The quality of the fits are similar to those presented in our previous work [9].

To determine the uncertainty in the polarisability difference, a jackknife error estimate is performed. A second-order jackknife is used to obtain uncertainties on the correlation functions and correlation function ratios. Uncertainties for fit values such as the magnetic polarisability energy shift for each field strength are obtained from individual first-order jackknife sub-ensembles. Finally, the fit of the energy shifts as a function of field strength is repeated on each jackknife sub-ensemble and the error on the ensemble average calculated as the jackknife error.

TABLE II. Details of the  $32^3 \times 64$  PACS-CS ensembles used in this work. The lattice spacing of each ensemble is set using the Sommer scale with  $r_0 = 0.4921(64)(+74)(-2)$  fm. In all cases  $\kappa_s^{\text{sea}} = 0.13640$  and  $\kappa_s^{\text{val}} = 0.13665$  [17].  $N_{\text{con}}$  describes the number of configurations.

$m_\pi^{\text{PACS}}$ (MeV)	$\kappa_{ud}$	$a$ (fm)	$N_{\text{con}}$
701	0.13700	0.1022(15)	399
570	0.13727	0.1009(15)	397
411	0.13754	0.0961(13)	449
296	0.13770	0.0951(13)	399

## VII. SIMULATION DETAILS

The details of the lattice simulation mirror those of our preceding work [9]. We reiterate the important details here.

### A. Lattice Actions

The four gauge ensembles used in this work are the four heaviest 2+1-flavour dynamical gauge configurations provided by the PACS-CS collaboration [18] through the International Lattice Data Grid (ILDG) [19]. The configurations have a range of degenerate up and down quark masses while the strange quark mass is fixed. The Iwasaki gauge action and the clover fermion action with  $C_{\text{SW}} = 1.715$  are used in generating the configurations. Details of the ensembles are summarised in Tab. II.

The ensembles were generated in the absence of a background magnetic field. As a result, the sea quarks are blind to the magnetic field and the ensembles may be regarded as electro-quenched. On the fifth, lightest ensemble, we encounter uncertainties which do not respond to increased statistics, hinting at an exceptional configuration problem associated with the electro-quenching of the light sea-quark sector. For this reason, it is omitted here.

Our valence fermion action matches the PACS-CS QCD action and includes the background field corrected clover term [20]. Periodic boundary conditions are used in the spatial directions. To avoid signal contamination from the backward propagating states, we use fixed boundary conditions in the temporal direction. The source is then placed at  $t = 16$ , one quarter of the total lattice time extent such that one is always well away from the fixed boundary.

### B. Baryon interpolating fields

The commonly used proton interpolating field in lattice QCD is given by [1]

$$\chi_p(x) = \epsilon^{abc} \left[ u^{aT} C \gamma_5 d^b(x) \right] u^c(x), \quad (34)$$

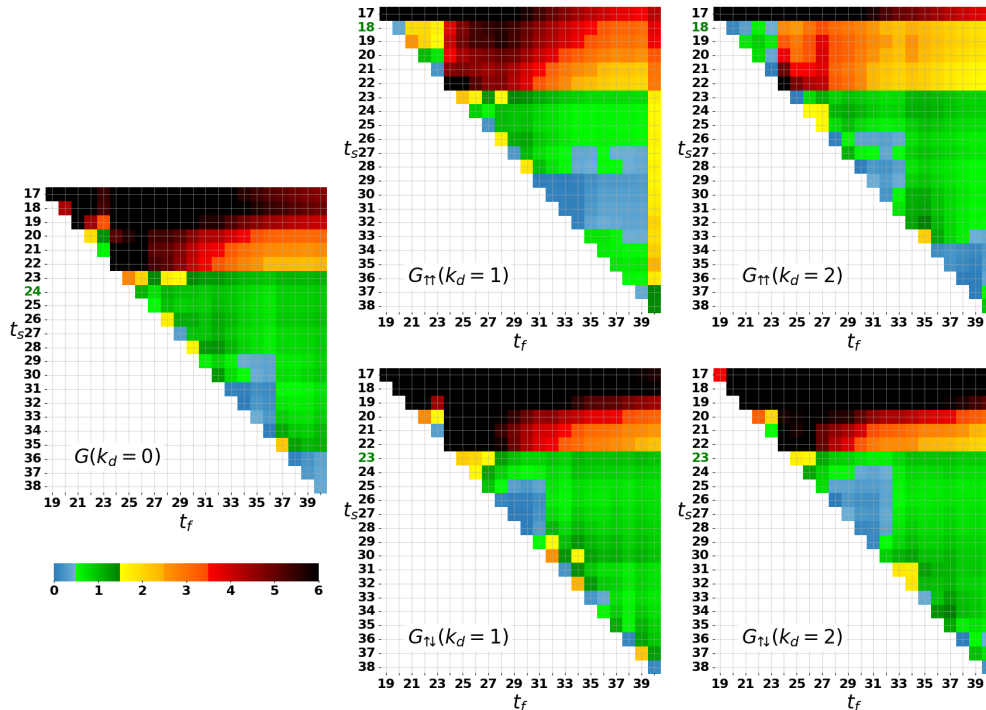


FIG. 2.  $\chi^2_{\text{dof}}$  heat maps for fits to  $\log G$  for all fit windows from  $t_s \rightarrow t_f$  of the aligned ( $\uparrow\uparrow$ ) and anti-aligned ( $\uparrow\downarrow$ ) correlators at each field strength of interest. The numbers in parentheses denote the field strength quanta governed by  $k_d$ . This example is a  $ddl$  baryon at  $\kappa = 0.13700$ ,  $m_\pi = 296$  MeV. The first time slice at which single-state isolation has been reached is highlighted green.

where  $C$  is the charge-conjugation matrix. We construct the fractionally charged baryons described in this work through use of this interpolating field, but provide the appropriate quark propagators to produce the desired particle. For example, in the construction of the  $ddh$  baryon, we provide a light quark propagator determined with the background field included in place of the doubly represented up quark and a heavy quark propagator determined at zero-field in place of the singly represented down quark.

Such interpolating fields, utilised purely with traditional gauge-covariant Gaussian smearing are ineffective at isolating the baryon ground state in a uniform background field [15, 21–23]. The uniform background field breaks the spatial symmetry and Landau-mode physics is present at both the quark and hadronic levels. This must be accommodated.

### C. Quark operators

As detailed in Ref. [9], we utilise asymmetric source and sink operators to maximise overlap of the lowest energy eigenstates of our baryons in magnetic fields. The operators we utilise also act to accommodate for the spatial symmetry and Landau-mode issues mentioned above.

Source and sink construction utilises links which are

smearing using stout link smearing [24]. 10 sweeps with isotropic smearing parameter  $\alpha_{\text{stout}} = 0.1$  are applied to spatially-oriented links.

We construct the quark source using three-dimensional, gauge-invariant Gaussian smearing [25]. At all quark masses  $\alpha = 0.7$  is used while the number of gauge invariant Gaussian smearing sweeps considered is quark mass dependent. Smearing is tuned to optimise the onset of early effective-mass plateaus with smaller numbers of sweeps associated with heavier quark masses. 150 to 350 sweeps are utilised.

The source construction is designed to provide a representation of the QCD interactions with the intent of isolating the QCD ground state. To encapsulate the quark-level physics of the electromagnetic and QCD interaction we utilise the eigenmode projection techniques demonstrated in Ref. [22], where a comprehensive explanation of the mechanisms may be found. A succinct summary of the approach is provided in Ref. [9].

The eigenmodes of the two-dimensional lattice Laplacian calculated on the  $SU(3) \times U(1)$  gauge links are used to produce a projection operator applied to the propagator at the sink. It is shown in Ref. [22], that including too few modes results in a noisy hadron correlation function in much the same manner as traditional sink smearing. As such, the number of modes is chosen to be large enough to minimise the noise of the correlation function,



but small enough to retain the focus on the aforementioned low-energy physics. The work of Ref. [22] found that  $n = 96$  modes provides balance to these two effects and we use this here.

#### D. Hadronic projection

The inclusion of the background magnetic field induces a change to the wave function of a charged baryon [26]. The quark level electromagnetic physics is highlighted by the eigenmode projection at the sink. However, we must also ensure that our operator has the appropriate electromagnetic characteristics on the hadronic level. By projecting final-state fractionally charged baryons to the state corresponding to the lowest-lying Landau level, we ensure  $n = 0$  in Eq. (19). The details of this projection are presented in Ref. [9].

Due to the colour singlet nature of the baryon, we need only project the eigenmodes of the U(1) Laplacian rather than the full lattice Laplacian used for the quark-propagator sink. These eigenmodes carry a degeneracy  $n$  in the finite volume of the lattice. For a baryon with charge  $q_B$  the degeneracy for the field strength  $k_d$  is

$$n = \left\lfloor k_d \frac{q_B}{q_d} \right\rfloor. \quad (35)$$

In this work, we consider fractionally charged baryons with hadronic charge  $q_B = -\frac{1}{3}$  and  $-\frac{2}{3}$ . At  $k_d = \pm 1$  their degeneracies will be 1 and 2 respectively, while at  $k_d = \pm 2$  their degeneracies will be 2 and 4 respectively. We utilise a linear combination of the degenerate eigenmodes which provides optimal overlap with the fermion source. The probability densities of these hadronic-level projection modes are shown in Fig. 3.

#### E. Statistics

As periodic boundary conditions are used in all four dimensions for the gauge field generation, one can exploit the associated translational invariance of the gauge fields. A quark source can be placed at any position on the lattice and then cycled with the gauge field to the standard source position of  $(x, y, z, t) = (1, 1, 1, N_t/4)$ , well away from any fermion action boundary conditions. This enables additional sampling of the full gauge field.

Further, the two-dimensional nature of the lattice Laplacian operator allows the eigenmodes for the sink projection to be re-used when the gauge field is cycled solely in the time direction. Hence, we increase our statistics on the PACS-CS ensembles by considering four random spatial sources at  $t = 16$ . The gauge field is then cycled in the temporal direction by an eighth of the lattice time extent (eight slices in our case) for each random source. This results in a further increase in statistics by a factor of eight. Together, random sources and time-direction cycles increase our statistics by a factor of 32.

These multiple samples are binned and averaged as a single configuration estimate in the error analysis.

### VIII. LATTICE RESULTS

In Figs. 4 and 5 we show the main results of this investigation. The indirect environment driven changes in the magnetic polarisability are illustrated in Fig. 4. From a quark model perspective this is the simple case where most effects cancel and changes are driven by changes in the octet-decuplet baryon mass splitting as in Eq. (15). The direct quark mass driven changes in the magnetic polarisability are illustrated in Fig. 5. In all cases, we have taken the difference with the lighter baryon subtracted from the heavier baryon.

In these figures, two datasets are illustrated. The points labelled "Ratio" are from the conventional analysis approach where reference to the correlation function ratio is used to identify fit plateaus. These results are complemented by the more rigorous results (offset for clarity) labelled "Corr." which are derived from strict requirements for single-state isolation in each of the underlying correlation functions involved in the ratio. The trends observed in both datasets agree. However, in some cases a loss of signal gives rise to very large uncertainties in the subtle polarisability changes for the Corr. method and we refer in these cases to the results determined in the Ratio method, as they may be more representative.

Let us commence with the general trends observed in the results. As the pion mass increases, all differences converge toward zero. This is to be expected as the strange quark mass is fixed for all PACS-CS ensembles. As the light  $d$  and  $l$  flavours approach the  $s$ -quark mass, the polarisability differences must vanish.

#### A. Environmental dependence in lattice QCD

Turning our attention to the environment driven changes in Fig. 4, we observe a clear environmental effect. We observe that increasing the mass of the spectator quark results in an increase of the magnetic polarisability. In Sec. III C 1, we showed that the quark model predicts such an effect for all four environmental considerations of Eq. (2). For example, consider Eq. (15)

$$\beta_{hhd} - \beta_{uld} = \frac{4}{9\pi} \left[ \frac{\mu_d^2}{m_{\Xi^*} - m_{\Xi}} - \frac{\mu_d^2}{m_{\Delta} - m_N} \right]. \quad (36)$$

Here, the environment effect is driven by the octet-decuplet mass splittings which govern the strength of the transition term. The larger magnetic polarisability of the heavier baryon seen in  $\Delta\beta$  is due to the smaller mass splitting for heavier baryons. In octet (decuplet) baryons the hyperfine attraction (repulsion) between the quarks is inversely proportional to the product of the constituent quark masses. As a result, the order of the octet-decuplet

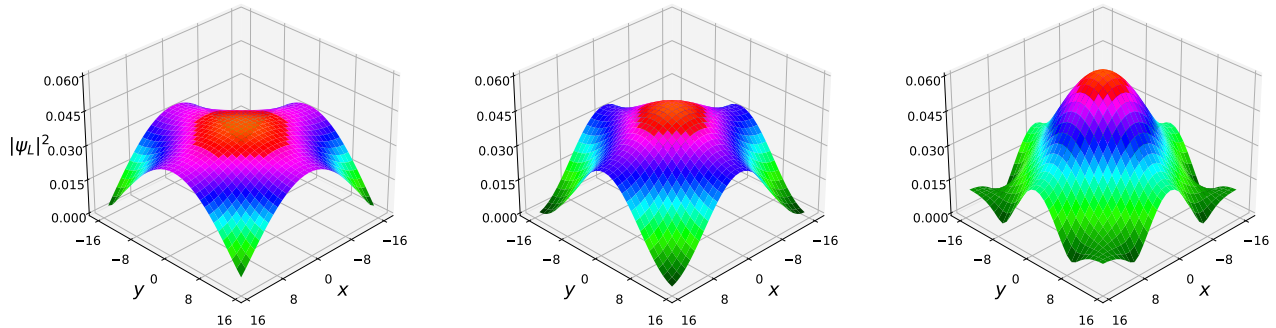


FIG. 3. Landau mode probability densities for fractional charge  $q_B = -\frac{1}{3}$  and  $-\frac{2}{3}$  baryons at our two lowest field strengths. Recalling  $n = |k_d q_B / q_d|$ , the  $n = 1$  (left),  $n = 2$  (centre) and  $n = 4$  (right) probability densities are illustrated for field strengths  $|k_d| = 1$  and  $2$ . The degeneracy of each mode is  $n$ .

mass splittings is  $N > \Sigma > \Xi > hhh$ . While the idea that heavier spectator quarks should give rise to larger magnetic polarisabilities may seem a little counterintuitive at first, the simple quark model provides a compelling explanation of the complex interactions of lattice QCD. It is satisfying that these early ideas founded in perturbation theory are manifest in the full nonperturbative formalism of lattice quantum field theory.

The quark model's suggestion of a simple effect based only on the octet-decuplet mass splitting does an impressive job of explaining the dependence, particularly for the doubly represented quark sector. The overestimate of the effect in the singly represented sector is interesting. It has long been known that the contributions of the singly represented quark flavour to baryon magnetic moments in lattice QCD is suppressed relative to constituent quark model predictions [1, 27]. However, this suppression was not observed in the effective quark moments of the  $\gamma N \rightarrow \Delta$  electromagnetic transition [3]. It would be interesting to revisit these early ideas drawing on modern lattice QCD techniques.

## B. Direct quark mass dependence in lattice QCD

In the case of the direct quark mass effect, we now know that increasing the mass of the charged quark of interest results in a decrease in the magnetic polarisability. Intuitively this is a comfortable result. However, the quark model presents a more complex competition of contributions.

Recall the discussion around Eq. (16)

$$\beta_{Us} - \beta_{Ud} = \frac{4}{9\pi} \left[ \frac{\mu_s^2}{m_{\Sigma^*} - m_{\Sigma}} - \frac{\mu_d^2}{m_{\Delta} - m_N} \right] - \left[ \frac{\alpha q_s^2}{6 m_h} \langle r^2 \rangle_h - \frac{\alpha q_d^2}{6 m_l} \langle r^2 \rangle_l \right], \quad (37)$$

in Sec. III C 2. As the constituent quark moments (Eq. (5)) are inversely proportional to quark mass, in-

creasing the quark mass decreases their contributions, which are squared in the transition term of the magnetic polarisability. In contrast, octet-decuplet mass splittings act in the opposite manner to increase the magnitude of the transition term, as it did in the environmental case above. Moreover the sign of the quark distribution term contributions also act to enhance the magnetic polarisability. However, the lattice QCD results now indicate the magnetic polarisability is suppressed as the quark mass of the active sector is increased, making the decrease in the constituent quark magnetic moment the dominant effect.

With regard to the singly represented quark sector results in the upper panel of Fig. 5, we once again observe an overestimate of the effect in the quark model. This is of a magnitude similar to that observed for the singly represented quark sector in the environmental case.

The tension between these effects increases for the doubly-represented quark sector where the size of the quark distribution term doubles as in Eq. (37), but the sign of the magnetic polarisability difference in lattice QCD continues to show the same trend. However, the quark model predictions are significantly impacted. This leads to significant discrepancies for the direct quark mass driven differences in the doubly represented sector at the lightest quark masses considered where the enhanced quark distribution term  $\beta_2$  is now able to dominate the contributions of the mass splitting and quark moments in the quark model.

Clearly, there is present behaviour that the quark model fails to capture. An increase in the transition term,  $\beta_1$ , relative to the distribution term,  $\beta_2$ , could drive the model prediction back towards the lattice QCD results.

And given that the singly represented sector overestimates the direct quark mass effect, one needs to suppress the single quark transition moment. These effects are in accord with the results of lattice QCD calculations for octet-baryon magnetic moments [1, 27]. Given that the model draws on these for the transition matrix element, there is qualitative agreement on the manner in which to

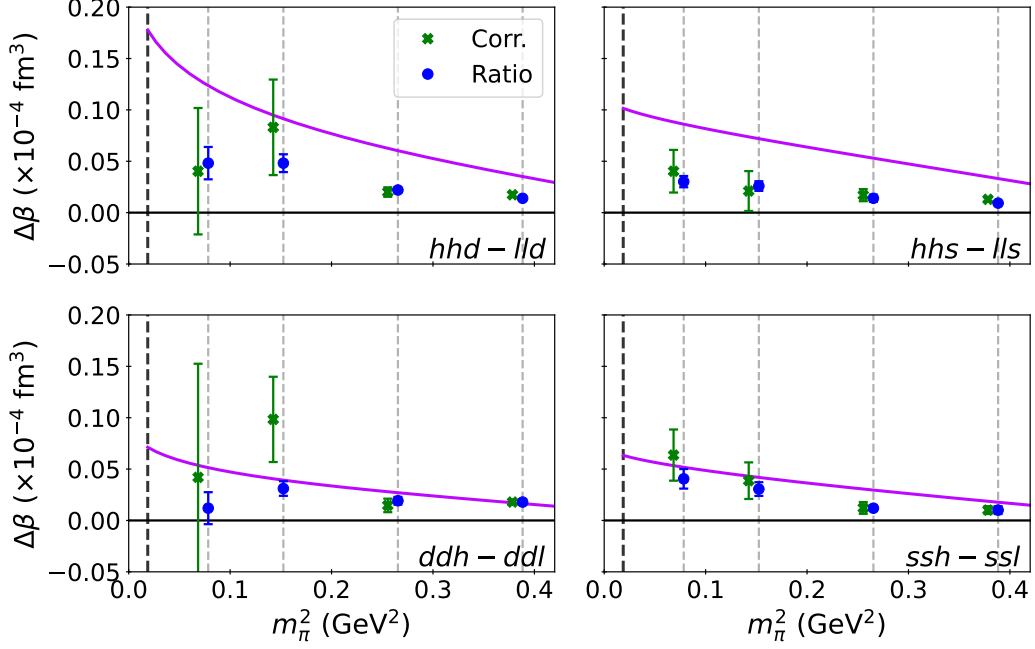


FIG. 4. Indirect environment driven changes in quark-sector contributions to octet baryon magnetic polarisabilities,  $\Delta\beta$ , for singly (upper) and doubly (lower) represented quark sectors. Results are plotted as a function of the pion mass governing the mass of the light  $d$  and  $l$  quarks. The labels in the lower-right of the panels indicate the magnetic polarisability difference illustrated. For example the upper left panel reports  $\Delta\beta = \beta_{hhd} - \beta_{ld}$ . The dataset labels "Ratio" and "Corr." are described in the text. The purple curve is the quark model prediction for the environment dependence as discussed in Sec. III C 1.

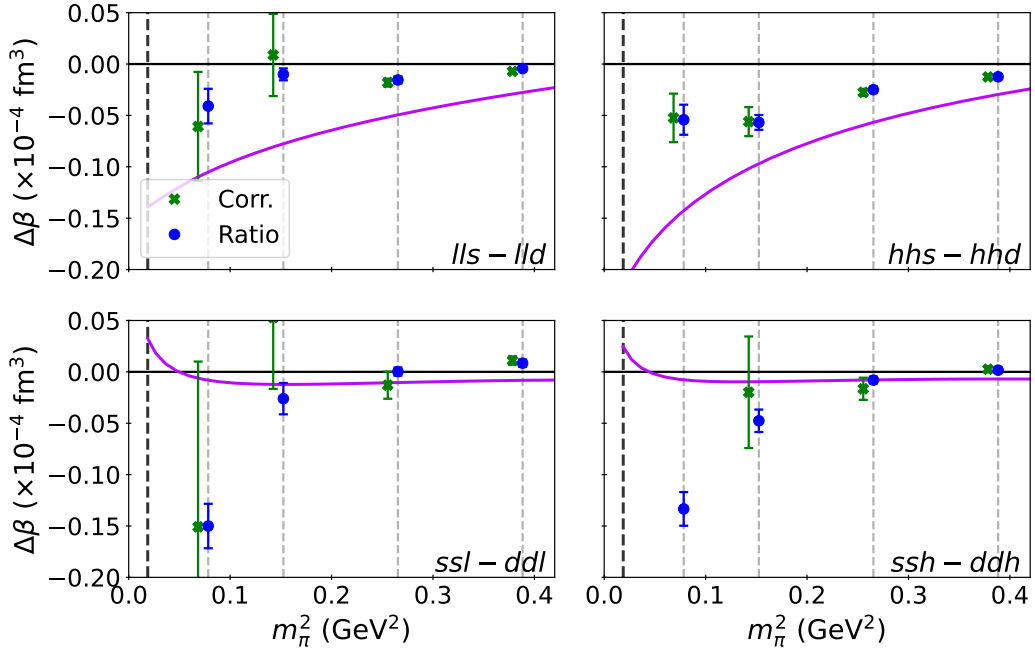


FIG. 5. Direct quark-mass driven changes in quark-sector contributions to octet baryon magnetic polarisabilities,  $\Delta\beta$ , for singly (upper) and doubly (lower) represented quark sectors. The presentation of the results is as in Fig. 4. Note, the missing data point at the lightest mass in the Corr. dataset for  $ssh - ddh$  is outside the scale presented at  $\Delta\beta = -0.41(14) \times 10^{-4} \text{ fm}^3$ .

TABLE III. Changes in the physical octet baryon magnetic polarisabilities due to an indirect environmental effect (top four) and a direct quark mass effect (bottom four). Physical baryon states where the effect will come into play are indicated. The  $u$  transitions column is obtained by replacing the active  $d$  quark with  $u$  quark. As there is no octet state composed of three heavy quarks, there is no corresponding change.

Difference	$d$ quark	$u$ quark	Sign
$hhd - lld$	$\Xi^- - p$	$\Xi^0 - n$	+
$hhs - lls$			+
$ddh - ddl$	$\Sigma^- - n$	$\Sigma^+ - p$	+
$ssh - ssl$			+
$lls - lld$	$\Sigma - p$		-
$hhs - hhd$			-
$ssl - ddl$	$\Xi^0 - n$		-
$ssh - ddh$			-

improve the quark model further.

Finally, we connect the implications of these results to the physical octet baryons in Tab. III. Here we list the physical states in which the differences studied herein can manifest. The first four rows of the table correspond to indirect environment effects which cause an increase in the magnetic polarisability when the mass of a spectator quark is increased. The bottom four rows correspond to the direct quark mass effect which causes a decrease in the magnetic polarisability as the active quark mass is increased.

The most interesting environment effects for understanding the ordering of  $n$ ,  $p$ , and  $\Sigma^+$  baryons are the  $hhd - lld$  and  $ddh - ddl$  which correspond to the differences in the contribution of the up quark in  $\Xi^0 - n$  and  $\Sigma^+ - p$  due to a change of environment. In both cases, the effect enhances the magnetic polarisability of the hyperon relative to the nucleon. Both differences also contain a direct mass effect on the other sector given by  $ssl - ddl$  and  $lls - lld$  respectively. In this case, the magnetic polarisability of the hyperon is suppressed. The opposing signs of the indirect environment effect and the direct mass effect highlights the complexity in understanding the magnetic polarisabilities of octet baryons. We now appreciate that the quark model underestimates the direct mass effect in the doubly represented sector, leaving the neutron polarisability higher than it should be. Thus we have found the origin of the chief discrepancy depicted in Fig. 1.

## IX. CONCLUSION

Introducing fractionally charged baryons to the background field formalism of lattice QCD, we have disclosed the individual quark sector contributions to the magnetic polarisabilities of the outer octet baryons. We have exposed a direct quark mass effect that acts to suppress the

magnetic polarisability as the quark mass increases. We have also observed an indirect environmental effect where the magnetic polarisability is enhanced as the mass of the spectator quark(s) are increased.

To gain an understanding of the underlying dynamics, we explored these direct and indirect effects in the context of a simple constituent quark model summarised in Eq. (3). The environmental effect appears as a relatively simple effect and may be explained by the change in the octet-decuplet mass splitting in the transition term,  $\beta_1$ . The behaviour of the quark mass dependence is predicted to be more complex in the model with competition between the intrinsic constituent quark moment and the octet-decuplet baryon mass splitting in the transition term,  $\beta_1$ , and further contributions from the quark distribution term,  $\beta_2$ .

We now understand that it is the transition term of the polarisability,  $\beta_1$  of Eq. (3), that contains the physics that describes our lattice QCD observations. The direct quark mass effect observed in the lattice results can be associated with the reduction of the intrinsic constituent quark moment for increasing quark mass, and this moment is squared in the numerator of  $\beta_1$ . The indirect effect observed in the lattice results can be associated with the reduction of the octet-decuplet mass splitting in the denominator of  $\beta_1$ , acting to enhance the magnetic polarisability as the quark mass increases and hyperfine effects separating the octet and decuplet baryon masses are suppressed.

We were not able to identify an equally important role for the quark distribution term of  $\beta_2$ . In fact its enhancement in the direct quark mass effect in the double-represented quark sector is problematic and hides the important effect of the transition term. It is the distribution term,  $\beta_2$ , that leaves the neutron magnetic polarisability high relative to the  $p$  and  $\Sigma^+$  polarisabilities and the lattice QCD results.

It would be interesting to perform a modern lattice QCD study of the effective quark moments of octet and decuplet baryons and their electromagnetic transitions to gain more precise insight into this physics driving direct and indirect environmental effects in baryon magnetic polarisabilities. Similarly, it will be advantageous to address the exceptional configuration problem encountered at light quark masses, opening the opportunity to explore the role of chiral physics. A first step would be to perform a filtering of the exceptional configurations to establish that the problem is understood. Longer term approaches could involve the use of chiral fermion actions to avoid problematic additive mass renormalisations. Alternatively, one could employ more efficient fermion actions and include the electric charges of the dynamical sea quarks such that they may correctly respond to the presence of a background magnetic field.

The results presented herein are founded on the PACS-CS ensembles of Ref. [18]. The ensembles are created by the PACS-CS collaboration, Aoki *et al.* and are avail-

able from <https://www2.jldg.org/>. The ensembles in question are part of the April 2009 release.

## ACKNOWLEDGMENTS

We thank the PACS-CS Collaboration for making their  $2 + 1$  flavour configurations available and the ongoing support of the International Lattice Data Grid (ILDG). Baryon correlation functions were constructed using the

COLA software library, developed at the University of Adelaide [28]. WK was supported by the Pawsey Supercomputing Centre through the Pawsey Centre for Extreme Scale Readiness (PaCER) program. This work was supported with supercomputing resources provided by the Phoenix HPC service at the University of Adelaide. This research was undertaken with the assistance of resources from the National Computational Infrastructure (NCI), which is supported by the Australian Government. This research is supported by Australian Research Council through Grants No. DP190102215 and No. DP210103706.

- 
- [1] D. B. Leinweber, R. M. Woloshyn, and T. Draper, Phys. Rev. D **43**, 1659 (1991).
- [2] D. B. Leinweber, T. Draper, and R. M. Woloshyn, Phys. Rev. D **46**, 3067 (1992), arXiv:hep-lat/9208025.
- [3] D. B. Leinweber, T. Draper, and R. M. Woloshyn, Phys. Rev. D **48**, 2230 (1993), arXiv:hep-lat/9212016.
- [4] D. B. Leinweber, Phys. Rev. D **45**, 252 (1992).
- [5] D. B. Leinweber, S. Boinepalli, I. C. Cloet, A. W. Thomas, A. G. Williams, R. D. Young, J. M. Zanotti, and J. B. Zhang, Phys. Rev. Lett. **94**, 212001 (2005), arXiv:hep-lat/0406002.
- [6] D. Djukanovic, K. Ottnad, J. Wilhelm, and H. Wittig, Phys. Rev. Lett. **123**, 212001 (2019), arXiv:1903.12566 [hep-lat].
- [7] C. Alexandrou, S. Bacchio, M. Constantinou, J. Finkenrath, K. Hadjiyiannakou, K. Jansen, and G. Koutsou, Phys. Rev. D **101**, 031501 (2020), arXiv:1909.10744 [hep-lat].
- [8] F. E. Close, *An Introduction to Quarks and Partons* (Academic Press, 1979).
- [9] T. Kabelitz, R. Bignell, W. Kamleh, and D. Leinweber, Phys. Rev. D (2024).
- [10] F. Gross *et al.*, Eur. Phys. J. C **83**, 1125 (2023), arXiv:2212.11107 [hep-ph].
- [11] R. L. Workman *et al.* (Particle Data Group), PTEP **2022**, 083C01 (2022).
- [12] A. Walker-Loud, PoS **LATTICE2013**, 013 (2014), arXiv:1401.8259 [hep-lat].
- [13] F. M. Stokes, W. Kamleh, and D. B. Leinweber, Phys. Rev. D **102**, 014507 (2020), arXiv:1907.00177 [hep-lat].
- [14] G. Martinelli, G. Parisi, R. Petronzio, and F. Rapuano, Phys. Lett. B **116**, 434 (1982).
- [15] T. Primer, W. Kamleh, D. Leinweber, and M. Burkardt, Phys. Rev. D **89**, 034508 (2014), arXiv:1307.1509 [hep-lat].
- [16] S. R. Beane *et al.* (NPLQCD, QCDSF), Phys. Rev. D **103**, 054504 (2021), arXiv:2003.12130 [hep-lat].
- [17] B. J. Menadue, *A Study of the  $\Lambda(1405)$  in Lattice QCD*, Ph.D. thesis, Adelaide U. (2018).
- [18] S. Aoki *et al.* (PACS-CS), Phys. Rev. D **79**, 034503 (2009), arXiv:0807.1661 [hep-lat].
- [19] F. Di Renzo, in *40th International Symposium on Lattice Field Theory* (2024) arXiv:2401.14752 [hep-lat].
- [20] R. Bignell, W. Kamleh, and D. Leinweber, Phys. Rev. D **100**, 114518 (2019), arXiv:1910.14244 [hep-lat].
- [21] A. Deshmukh and B. C. Tiburzi, Phys. Rev. D **97**, 014006 (2018), arXiv:1709.04997 [hep-ph].
- [22] R. Bignell, W. Kamleh, and D. Leinweber, Phys. Rev. D **101**, 094502 (2020), arXiv:2002.07915 [hep-lat].
- [23] F. Bruckmann, G. Endrodi, M. Giordano, S. D. Katz, T. G. Kovacs, F. Pittler, and J. Wellenhofer, Phys. Rev. D **96**, 074506 (2017), arXiv:1705.10210 [hep-lat].
- [24] C. Morningstar and M. J. Peardon, Phys. Rev. D **69**, 054501 (2004), arXiv:hep-lat/0311018.
- [25] S. Gusken, Nucl. Phys. B Proc. Suppl. **17**, 361 (1990).
- [26] D. S. Roberts, P. O. Bowman, W. Kamleh, and D. B. Leinweber, Phys. Rev. D **83**, 094504 (2011), arXiv:1011.1975 [hep-lat].
- [27] S. Boinepalli, D. B. Leinweber, A. G. Williams, J. M. Zanotti, and J. B. Zhang, Phys. Rev. D **74**, 093005 (2006), arXiv:hep-lat/0604022.
- [28] W. Kamleh, PoS **LATTICE2022**, 339 (2023), arXiv:2302.00850 [hep-lat].